Published in final edited form as:

Biochemistry. 2012 November 6; 51(44): 8844–8855. doi:10.1021/bi301135b.

Human UDP-α-D-xylose Synthase and *Escherichia coli* ArnA Conserve a Conformational Shunt That Controls Whether Xylose or 4-Keto-Xylose Is Produced

Samuel J. Polizzi[†], **Richard M. Walsh Jr.**[†], **William B. Peeples**[†], **Jae-Min Lim**[‡], **Lance Wells**[†,§], and **Zachary A. Wood**[†,*]

[†]Department of Biochemistry and Molecular Biology, University of Georgia, Athens, Georgia 30602, United States

[§]Complex Carbohydrate Research Center, University of Georgia, Athens, Georgia 30602, United States

[‡]Department of Chemistry, Changwon National University, 9-Sarim, Changwon, Gyeongnam 641-773, South Korea

Abstract

Human UDP-α-D-xylose synthase (hUXS) is a member of the short-chain dehydrogenase/reductase family of nucleotide-sugar modifying enzymes. hUXS contains a bound NAD^+ cofactor that it recycles by first oxidizing UDP-α-D-glucuronic acid (UGA), and then reducing the UDP-α-D-4-ketoxylose (UX4O) to produce UDP-α-D-xylose (UDX). Despite the observation that purified hUXS contains a bound cofactor, it has been reported that exogenous NAD^+ will stimulate enzyme activity. Here we show that a small fraction of hUXS releases the NADH and UX4O intermediates as products during turnover. The resulting apoenzyme can be rescued by exogenous NAD^+, explaining the apparent stimulatory effect of added cofactor. The slow release of NADH and UX4O as side products by hUXS is reminiscent of the *Escherichia coli* UGA decarboxylase (ArnA), a related enzyme that produces NADH and UX4O as products. We report that ArnA can rebind NADH and UX4O to slowly make UDX. This means that both enzymes share the same catalytic machinery, but differ in the preferred final product. We present a bifurcated rate equation that explains how the substrate is shunted to the distinct final products. Using a new crystal structure of hUXS, we identify the structural elements of the shunt and propose that the local unfolding of the active site directs reactants toward the preferred products. Finally, we present evidence that the release of NADH and UX4O involves a cooperative conformational change that is conserved in both enzymes.

Graphical Abstract

[*]**Corresponding Author**. Phone: 706-583-0304, fax: 706-542-1783, zac@bmb.uga.edu.

ASSOCIATED CONTENT

Accession Codes

The atomic coordinates and structure factors for the open form of hUXS have been deposited in the Protein Data Bank (PDB ID code 4GLL).

The authors declare no competing financial interest.

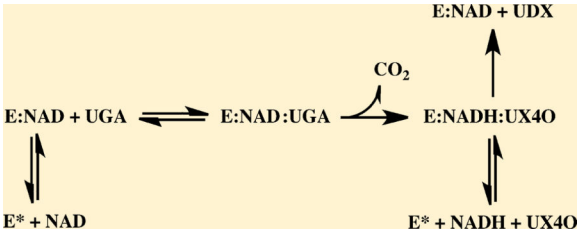

Proteoglycans act as receptors for growth factors and are essential for cell proliferation, migration and adhesion.[1–3] Disrupting proteoglycan biosynthesis can attenuate tumor growth and progression; thus controlling proteoglycan biosynthesis is a promising strategy for treating cancer.[2–5] The biosynthesis of most proteoglycans begins with the covalent attachment of xylose to the hydroxyl of a serine.[6–8] In mammals, xylose is also used in non-mucin O-glycosylation of key regulatory proteins such as Notch and α-dystroglycan that play important roles in cancer progression and metastasis.[9–12] The nucleotide sugar donor that initiates xylose transfer is produced by UDP-α-D-xylose synthase (UXS; E.C. 4.1.1.35), a member of the short-chain dehydrogenase/reductase (SDR) family. Understanding the mechanism of UXS may contribute to the design of strategies that will slow or prevent metastasis.

SDR enzymes share a common catalytic domain containing a Rossmann fold for binding the NAD^+ cofactor.[13] UXS is further classified as an ‘extended’ SDR due to an inserted nucleotide sugar binding domain (NSBD).[14,15] The extended SDR subfamily includes nucleotide sugar epimerases, dehydratases and decarboxylases, all of which use a similar NAD^+-dependent mechanism. The recent crystal structure of human UXS (hUXS) in complex with NAD^+ and UDP has shed light on the mechanism (Figure 1).[15] Briefly, hUXS uses a bound NAD^+ cofactor to oxidize of the C4′ atom of UDP-α-D-glucuronic acid (UGA) to produce UDP-α-D-4-keto-glucuronic acid. The unstable β-keto-acid intermediate decarboxylates to form the more stable UDP-α-D-4-keto-xylose (UX4O). Finally, hUXS uses the NADH cofactor produced in the first step to reduce the UX4O intermediate to UDP-α-D-xylose (UDX). hUXS purifies with a bound cofactor and therefore has no requirement for additional NAD^+.[16] Despite this observation, several reports have demonstrated that adding exogenous NAD^+ can stimulate UXS activity by 10–104%.[15,17–21] This stimulation has been attributed to a significant contamination of apoenzyme in purified UXS.[15,17]

We present evidence that the stimulatory effect of exogenous NAD^+ is due to the accumulation of apo-hUXS during catalytic turnover. We show that the hUXS mechanism shunts UGA into two different paths: (i) the slow production of NADH and UX4O, or (ii) the preferred conversion to UDX. The first path results in an inactive apoenzyme that can be rescued by exogenous NAD^+. In contrast to hUXS, the homologous UGA decarboxylase domain of *Escherichia coli* ArnA uses NAD^+ as a cosubstrate and releases NADH and UX4O as products (Figure 1).[22,23] We show that cofactor binding in UXS and ArnA invokes a conserved, cooperative conformational change. Interestingly, ArnA conserves the bifurcated mechanism of hUXS and can produce UDX, albeit rather inefficiently. Using a new crystal structure of hUXS, we identify the flexible active site elements that contribute to the UX4O and NADH shunt. We present a model for this bifurcated mechanism that

explains the stimulatory effect of exogenous NAD^+ on hUXS and the production of UDX by ArnA.

MATERIALS AND METHODS

Protein Purification

A hUXS construct lacking the 84 residue N-terminal transmembrane domain was designed based on the crystal structure of hUXS in complex with UDP (PDB entry 2B69)[15] and then expressed and purified as previously reported.[16] It has been suggested that heterologously expressed hUXS contains a significant fraction of apoenzyme. We used the following assay to determine the stoichiometry of hUXS:NAD^+ in our expressed protein. The absorbance spectrum of purified, total hUXS (hUXS + NAD^+) was recorded on an Agilent 8453 UV–vis spectrophotometer (Figure 2A). To quantitate the amount of NAD^+, the sample was recovered from the cuvette, boiled for 5 min and centrifuged to remove protein. The absorbance spectrum of the supernatant containing the cofactor was recorded and quantitated using the molar absorptivity of NAD^+ (ε_{260} = 17400 M^{-1} cm^{-1}).[24] To quantitate the amount of pure protein, the NAD^+ supernatant spectrum was subtracted from that of the total protein (hUXS + NAD^+), and the resulting spectrum (protein alone) was quantitated using the molar absorptivity of hUXS calculated with ProtParam (ε_{280} = 37360 M^{-1} cm^{-1}) (Figure 2A).[25] An expression construct (pMS159) containing the decarboxylase domain of *E. coli* ArnA (residues 306–660) was kindly provided by M. Sousa. This fragment has previously been shown to have the same decarboxylase activity as full length ArnA[22] and is simply referred to as ArnA throughout this work. ArnA was expressed in BL21 cells grown to an OD_{600} ~1.3 at 37 °C in Terrific Broth containing 50 μg/mL Kanamycin (Research Products International). Expression was induced after cooling the cultures to 15 °C and adding IPTG (Research Products International) to a final concentration of 2 mM. Cells were harvested after 24 h. Purification and cleavage of His-tagged ArnA were performed as previously described for hUXS.[16]

Capillary Electrophoresis

The products of hUXS and ArnA were resolved using a G1600 3D capillary electrophoresis system (Agilent Technologies). Reactions were quenched by plunging in liquid nitrogen and extracted with 1:1 v/v chloroform while thawing. Capillary zone electrophoresis (CZE) of the aqueous layer was performed in a fused-silica capillary (56 cm × 50 μm) with an extended light path using 20 mM borate pH 9.3 as the background electrolyte at 22 kV and 18 °C. Absorbance spectra were collected between 200 and 400 nm and products were identified by comigration with known standards. The UX4O standard was a kind gift of M. Bar-Peled. Product peaks were manually integrated using Agilent CE ChemStation software Rev. B.03.01, and scaled using an internal caffeine standard (5 mM; Sigma-Aldrich) for progress curves. UX4O and NADH peaks were converted to molar concentrations using the 260 nm molar absorption coefficients 9820 M^{-1} cm^{-1} and 14100 M^{-1} cm^{-1}, respectively.[24]

HPLC Purification and Collision Induced Dissociation (CID) Mass Spectrometry

UX4O and UDX were purified using a Dionex HPLC equipped with an AD20 absorbance detector and a GP40 gradient pump. The hUXS reaction was resolved on a CarboPac

analytical column (4 mm × 250 mm) using a linear ammonium formate gradient flowing at 1 mL/min over 25 min. Fractions were collected and products were confirmed using CZE as described above. Purified UX4O and UDX were identified using a hybrid linear ion trap-Fourier transform mass spectrometer (LTQ-Orbitrap XL ETD, Thermo-Fisher, San Jose, CA). UDP-sugars were dissolved in 50 μL of sample solution: 15 μL of 100% methanol followed by the addition of 35 μL of 1 mM NaOH in 50% methanol and injected directly into the mass spectrometer using a nanospray ion source with a fused-silica emitter (360 × 75 × 30 μm, SilicaTip, New Objective) at 2.0 kV capillary voltage, 240 °C capillary temperature, and a syringe flow rate of 0.5 μL/min. The $FTMS^2$ (Fourier transform mass spectrometry) spectra at 60 000 resolution was collected at 36% collision-induced dissociation (CID) from the sodiated mass of UDP-xylose (602.9992 *m/z*) with 2.0*m/z* isolation width. The $FTMS^3$ was performed on a b3-H (358.926 *m/z*) fragment ion with 36% CID and 2.0 *m/z* isolation width. For analysis of UDP-4-keto-xylose, a MS/MS spectrum of ion trap mass spectrometry (ITMS) was acquired at 36% CID and 0.8 *m/z* isolation width from the sodiated mass of UDP-4-keto-xylose (600.9835 *m/z*).

Enzyme Assays

hUXS (1 mg/mL) was assayed in standard reaction conditions (50 mM Tris pH 8.0, 10 mM DTT and 1 mM EDTA) at 25 °C. Initial velocities with variable NAD^+ (0.05–5 mM; Sigma-Aldrich) and saturating UGA (1 mM), or variable UGA (0.005–5 mM) with saturating NAD^+ (5 mM) were measured by monitoring NADH absorbance at 340 nm with an Agilent 8453 UV–vis spectrophotometer equipped with a Peltier temperature controller set at 25 °C. The NADH concentration was calculated using the 340 nm molar absorptivity coefficient 6220 M^{-1} cm^{-1}.[24] Initial velocities for ArnA (0.5 mg/mL) were measured under the same buffer and temperature conditions as hUXS, with variable NAD^+ (0.05–15 mM) and saturating UGA (5 mM), or variable UGA (0.05–5 mM) with saturating NAD^+ (5 mM). Initial velocities were fit to the bifurcated steady state rate equation (derived below) using nonlinear regression in Prism (GraphPad Software, Inc.).

Scheme 1 illustrates the bifurcated steady state kinetics of hUXS with variable cofactor NAD^+ (A) and saturating substrate UGA (B).

E* and EA represent the apo and cofactor-bound forms of the enzyme, respectively. We assume that the concentration of EA is negligible in the presence of saturating [B] and EAB is the relevant Michaelis complex. The divergent pathways that yield the reduced product UDX (P), or release the reaction intermediates NADH (Q) and UX4O (R) are governed by the distinct rate constants, k_2 and k_3, respectively. The fraction of [EAB] that produces and releases the intermediates during each catalytic cycle is

$$f_{\text{release}} = \frac{k_3}{k_2 + k_3}[\text{EAB}] \quad (1)$$

The rate equation for the release of the intermediate products Q and R is

$$V_0(\mathrm{A}) = k_3 f_{\mathrm{release}} = \frac{k_3 k_3}{k_2 + k_3}[\mathrm{EAB}] \quad (2)$$

To solve this equation, we assume the steady state condition 3 and express [E*] in terms of total enzyme 4:

$$k_1[\mathrm{E}^*][\mathrm{A}] = k_{-1}[\mathrm{EAB}] + k_2[\mathrm{EAB}] + k_3[\mathrm{EAB}] \quad (3)$$

$$[\mathrm{E}^*] = [\mathrm{E}]_{\mathrm{total}} - [\mathrm{EAB}] \quad (4)$$

Substitute 4 into 3 and simplify:

$$k_1([\mathrm{E}]_{\mathrm{total}} - [\mathrm{EAB}])[\mathrm{A}] = (k_{-1} + k_2 + k_3)[\mathrm{EAB}] \quad (5)$$

Solve for [EAB] and rearrange,

$$[\mathrm{EAB}] = \frac{k_1[\mathrm{E}]_{\mathrm{total}}[\mathrm{A}]}{(k_{-1} + k_2 + k_3) + k_1[\mathrm{A}]} = \frac{[\mathrm{E}]_{\mathrm{total}}[\mathrm{A}]}{[(k_{-1} + k_2 + k_3)/k_1] + [\mathrm{A}]}; \mathrm{let} \frac{(k_{-1} + k_2 + k_3)}{k_1} = K_{\mathrm{M}}^{\mathrm{app}} \quad (6)$$

$$[\mathrm{EAB}] = \frac{[\mathrm{E}]_{\mathrm{total}}[\mathrm{A}]}{K_{\mathrm{M}}^{\mathrm{app}} + [\mathrm{A}]} \quad (7)$$

Substitute 7 into 2:

$$V_0(\mathrm{A}) = \frac{[(k_3 k_3)/(k_2 + k_3)]\,[E]_{\mathrm{total}}[\mathrm{A}]}{K_{\mathrm{M}}^{\mathrm{app}} + [A]} = \frac{V_{\mathrm{max}}^{\mathrm{app}} + [A]}{K_{\mathrm{M}}^{\mathrm{app}} + [A]} \quad (8)$$

Finally, we express the rate equation in the more general form to accommodate cooperativity by assuming that the Hill coefficient (*h*) may not be unity:

$$V_0(A) = \frac{V_{\mathrm{max}}^{\mathrm{app}}[\mathrm{A}]^h}{(K_{\mathrm{M}}^{\mathrm{app}})^h + [\mathrm{A}]^h} \quad (9)$$

Crystallization, Data Collection and Refinement

hUXS crystals were obtained with precipitant containing 1.3 M ammonium sulfate, 0.1 M magnesium formate and 0.15% PEG at 26 °C using the hanging-drop vapor-diffusion

method. Rod-shaped crystals took 7 to 21 days to appear and grew to approximately 0.15 mm in length. hUXS crystallized in space group $P3_221$ with unit cell dimensions a = 125.6 Å, c = 98.9 Å and two molecules per asymmetric unit. For data collection, crystals were cryoprotected by passing through a mixture of paratone/paraffin (50:50 ratio) and then plunged into liquid nitrogen. Data were collected on beamline 8.2.1 at the Advanced Light Source (ALS, Berkeley, CA) using an ADSC Q210 detector. Data sets were processed with both the HKL suite of programs[26] and XDS.[27] Data collection statistics are reported in Table 1.

The structure of hUXS was solved by molecular replacement using the CNS suite of programs.[28] The crystal structure of a hUXS monomer (PDB entry 2B69) was used as a search model. For molecular replacement, the ligands and waters were removed from the search model, and 5% of the data were set aside for cross validation.[29] Two monomers were placed in the asymmetric unit to form the complete biological dimer. Iterative cycles of model refinement and manual rebuilding were carried out using REFMAC[30] and Coot,[31] respectively. Model refinement statistics are reported in Table 1.

Structural Analyses

Structural comparisons were performed using the atomic coordinates of unliganded hUXS (PDB entry 4GLL), the hUXS:UDP complex (2B69),[15] apo-ArnA (2BLL),[32] and the decarboxylase domain of the full length ArnA:ATP:UGA complex (1Z7E).[33] Main chain B-factors were averaged with BAVERAGE.[30] Solvent accessible surface area was calculated using AREAIMOL[30] with a probe radius of 1.4 Å. Sequence identities were calculated using NCBI-BLAST[34] and/ or DaliLite.[35] LIGPLOT[36] was used to analyze hydrogen bonding and packing interactions between hUXS and the bound ligands. Substrate induced conformational changes were analyzed using difference distance matrix analysis.[37] The NSBD rotation axis was generated using DYNDOM.[38] Structural figures were generated using Pymol (http://www.pymol.org).

RESULTS

Human UXS Releases the Reaction Intermediates NADH and UDP-4-keto-xylose

We expressed human UXS lacking the N-terminal membrane-spanning domain (hUXS; residues 85–420) as described elsewhere.[16] In our hands, recombinant hUXS purifies with the NAD^+ bound in stoichiometric amounts (see Methods). The average of three different protein preps yielded 1.07 ± 0.05 mol of NAD^+ per mol of protein (Figure 2A). Using CZE, we show that recombinant hUXS converts UGA to UDX without need of additional cofactor (Figure 2B). In the presence of exogenous NAD^+, two additional products are formed (Figure 2B). The first product was identified as NADH based on comigration with known standards and a characteristic absorbance spectrum (Figure 2C). The second product has a UV absorbance spectrum matching a UDP-sugar (Figure 2D). On the basis of molar absorptivity of uridine, the additional product is formed in stoichiometric amounts with NADH (1.1:1) and is consistent with a UDP containing reaction intermediate from the hUXS catalytic cycle (Figure 1). We postulated that the product was UX4O, since UDP-4-keto-glucuronic acid is a labile β-keto acid and would be expected to undergo

decarboxylation. In support of our hypothesis, the UDP-containing product comigrates with a UX4O standard during CZE (data not shown).

We used mass spectrometry to confirm the identity of the putative UX4O. The UDP-containing products were purified using HPLC. We identified fractions corresponding to UDX and UGA, but we did not detect a separate peak for UX4O (Figure 3A). We used the higher resolution of CZE to show UX4O comigrates with UDX during HPLC purification (Figure 3B). The HPLC purified UDX/UX4O fraction was analyzed with a hybrid linear ion trap-Fourier transform mass spectrometer (see Methods). Collision-induced dissociation mass spectroscopy (CID-MS^n) confirms that the HPLC fraction contains two species: UDX and UX4O. The major species is consistent with sodiated UDX cleaving along the glycosidic bond of uridine with hydrogen rearrangement (b4-H, 490.967 *m/z*) and the phosphoester bond of phosphate with rearrangement (b3-H, 358.926 *m/z* and b2-H, 256.978 *m/z* respectively) (Figure 3C). The minor species shows the same cleavage pattern as UDX, but with a mass reduced by 2Da (Figure 3D), consistent with the loss of two hydrogen atoms to form the C4′ ketone of UX4O.

hUXS and ArnA Conserve NAD^+ Substrate Cooperativity

Our observation that hUXS produces both UDX and the intermediates NADH and UX4O as terminal products indicates that the reaction mechanism is bifurcated (Figure 4A). The release of the reaction intermediates from hUXS is ~2 orders of magnitude slower than the production of UDX (specific activities of 3.45 ± 0.08 and 534 ± 29 nmol mg^{-1} min^{-1}, respectively). This means that the release of the NADH and UX4O intermediates only weakly competes with the synthesis of UDX. Still, to accurately describe the steady state kinetics of the slower NADH and UX4O release, we derived a bifurcated rate equation for fitting the substrate saturation curves (see Methods). The NAD^+-dependent substrate saturation curve for hUXS intermediate release is sigmoidal (Hill coefficient = 1.8) (Table 2), showing that cofactor binding to apo-hUXS (E*) is cooperative (Figure 4B). The UGA substrate saturation curve is also cooperative, albeit with a significantly lower Hill of 1.2 (Figure 4C). Next, we examined the *E. coli* UGA decarboxylase ArnA. ArnA conserves the first catalytic step with hUXS to produce NADH and UX4O as end products (Figure 1). Like hUXS, the steady state kinetics of ArnA also displays a strong NAD^+ dependent cooperativity (Hill = 1.7) (Figure 4D). The UGA substrate saturation curves show very little, if any, cooperativity in ArnA (Hill = 1.1) (Figure 4E).

ArnA Catalyzes UDP-Xylose Synthesis

On the basis of the similarities in structure and chemistry, we asked if ArnA has a bifurcated reaction mechanism (Figure 4A). Using CZE, we show that ArnA produces both UX4O and UDX (Figure 5A). The ArnA progress curves for UDX production display a distinctive lag in activity (Figure 5B). A lag in progress curves usually indicates the presence of a transient in the reaction and can be modeled using the equation:[39]

$$P = V_{SS} - (V_{SS} - V_i)(1 - e^{-t/\tau})\tau$$

where P is the product concentration at time, t, and τ is the half-life for the transition between the initial (V_i) and final steady state velocities (V_{ss}). The τ calculated from the UDX progress curve is coincident with the plateaus of NADH and UX4O and the depletion of UGA (Figure 5C). In addition, the final V_{ss} of UDX production is reflected in the depletion of UX4O and NADH. This supports a mechanism in which UX4O and NADH rebind to ArnA to produce UDX.

NAD$^+$ Is Buried in the Core of hUXS

We solved the crystal structure of hUXS at 2.5 Å resolution, revealing a dimer in the asymmetric unit (Figure 6A). The extreme N-terminus of both chains is disordered (residues 85–87), as is the C-terminus of chain A (395–420) and chain B (399–420). In addition, residues 166–170 are disordered in chain B. The equivalent residues in chain A form a helix that is buried in a crystal contact. Crystal lattice formation selects for stable conformations and is too weak to deform protein structures,[40,41] suggesting residues 166–170 are flexible in solution, and the helix we observe is a consequence of crystal packing (discussed below). The structure of hUXS is divided into a nucleotide sugar-binding domain (NSBD) and a catalytic domain (Figure 6A). Because the crystal structure of hUXS in complex with UDP as a substrate analogue (hUXS:UDP) has recently been described,[15] we will focus our analysis on the conformational changes associated with cofactor and substrate binding.

Recombinant hUXS crystallizes with the copurified NAD$^+$ cofactor bound (Figure 6). While no structures of *E. coli* ArnA contain NAD$^+$, one structure was solved with ATP bound as a cofactor analogue (PDB entry 1Z7E).[33] hUXS and *E. coli* ArnA share 28% sequence identity and superimpose 305 corresponding Cα atoms with an rmsd of 1.9 Å. The superposition shows that hUXS and ArnA bind cofactor in a similar binding cleft (Figure 6B). In hUXS, the *re* face of the nicotinamide ring is supported by packing interactions with the side chain and carbonyl oxygen of Ile258 (Figure 6C). ArnA conserves a surprisingly similar nicotinamide packing surface through an unorthodox substitution; Pro490 of ArnA is structurally equivalent to the nonisosteric Ile258 of hUXS (Figure 6C). To accomplish this, ArnA has undergone small structural rearrangements that shift the main chain Cα atom of Pro490 by ~1.2 Å relative to Ile258 in the hUXS structure. Recently, the Seattle Structural Genomics Center for Infectious Disease deposited the atomic coordinates of an annotated UGA decarboxylase from *Burkholderia pseudomallei* (PDB entry 3SLG) which conserves the same proline packing surface associated with the nicotinamide binding (not shown).

The adenosyl base of the cofactor is significantly shifted between the hUXS and ArnA structures, primarily due to differences in $Loop_{120–124}$ (hUXS numbering) (Figure 6D). In hUXS, the amide group of Asn120 packs on top of the adenylate base, and Thr123 and Gly124 contribute a total of three hydrogen bonds. In addition, Thr178 and His267 contribute hydrogen bonds to the N6 of the adenylate base and α-phosphate, respectively (Figure 6D). In hUXS, only ~4% of the cofactor is exposed to solvent. The $Loop_{120–124}$, Thr178 and His267 interactions are not conserved in ArnA (Figure 6D,E). As a consequence, ArnA binds the adenosine base and ribosyl in an altered conformation and exposes more of the adenylate to solvent (Figure 6B,D). The remaining hydrogen bonds and packing interactions with the cofactor are conserved in both hUXS and ArnA (Figure 6E).

Modeled GlcA Binding in the hUXS Active Site

To better understand the conformational changes associated with NADH and UX4O release, we modeled GlcA in the hUXS active site. As a starting model, we used the crystal structure of a hUXS complex containing UDP and NAD^+ (PDB entry 2B69).[15] The chemistry of hydride transfer provides restraints for modeling a likely binding mode for GlcA in the active site, specifically: (i) hydride transfer to NAD^+ requires that the carbon and hydrogen atoms of the C4′ position of GlcA are almost in-line with the C4 atom of the nicotinamide (C4′–H′–C4 angle slightly less than 180°);[42] (ii) the angle between the GlcA C4′ and the nicotinamide C4–N1 atoms varies between 81° to 145°;[43–45] and (iii) the distance between the C4′–C4 atoms should be approximately 3.5 Å.[44,45] Using only these constraints, we modeled the position and orientation of GlcA such that the C1′ atom could bond with the β-phosphate of UDP in the hUXS:UDP structure (Figure 7A). Support for our modeled conformation can be seen in the ordered water structure of the active site, which closely approximates the volume, shape and hydrogen bonding requirements of GlcA (Figure 7A). Similarly ordered water structures are often seen compensating for missing sugar molecules in carbohydrate binding enzymes.[46–48] Even though no side chains were adjusted in this modeling exercise, the GlcA conformation is consistent with the active site architecture and hydrogen bonding requirements.

Substrate Binding in hUXS Reveals Structural Elements Involved in the Release of Reaction Intermediates

Our crystal structure represents the NAD^+-bound, ‘open’ conformation of hUXS. A comparison with the ‘closed’ hUXS:UDP structure shows that UDP binding causes the NSBD to undergo a ~34° domain rotation to close the active site (Figure 7B). The superposition identifies three flexible regions at the NSBD/catalytic domain junction that contribute to substrate and cofactor retention: (i) $Helix_{165–168}$, (ii) $Loop_{159–164}$ and (iii) $Loop_{266–272}$ (Figure 7C). $Helix_{165–168}$ undergoes a disorder-to-order transition to fold over the sugar substrate and close off the active site from solvent (Figure 7C). A similar substrate induced folding of the equivalent helix in dTDP-glucose 4,6-dehydratase (RmlB) has been reported.[45] $Loop_{159–164}$ folds over and retains the cofactor. $Loop_{159–164}$ is more rigid when $Helix_{165–168}$ folds, based on a 70% reduction in Cα *B*-factors between chain A and B in our hUXS structure (average *B*-factors for entire chains 39.5 and 39.9 $Å^2$, respectively). $Loop_{266–272}$ is part of the NSBD, and shifts to shield the substrate and cofactor as the domain rotates to the closed conformation. This shift breaks a hydrogen bond between the imidazole of His263 and the α-phosphate, and forms a new hydrogen bond between the guanidinium of Arg272 and the β-phosphate of NAD^+ (Figure 7C).

The ArnA:ATP Structure Reveals an Induced-Fit Conformational Change Associated with Cofactor Binding

All of the conformational changes associated with substrate binding in hUXS are conserved in ArnA (see previous section). In addition, ArnA allows us to examine changes associated with the transition from the apo- to the holoenzyme. A comparison of the catalytic domains from apo-ArnA and the ArnA:ATP:UGA ternary complex (PDB entries 2BLL and 1Z7E, respectively) identifies three regions that flank the NAD^+-binding site and shift in response

to cofactor binding (Figure 8). First, the N-terminus of $Helix_{326–337}$ shifts by 2.2 Å to facilitate the conserved interaction between the Rossmann GxxGxxG motif and the pyrophosphate of NAD^+. A second structural element, $Loop_{347–349}$, moves 2.6 Å toward the cofactor binding site to facilitate conserved hydrogen bonds between Asp347 (Asp119 in hUXS) and the C2′ and C3′ hydroxyls of the adenine ribose (Figures 6E and 8). $Loop_{347–349}$ also shifts toward the cofactor binding pocket to interact with the adenosine moiety. Finally, the N-terminal loop of $Helix_{373–381}$ shifts away from the dimer interface by 2.8 Å and maintains packing interactions with $Loop_{347–349}$. The side chain of Asp368 (Asp144 in hUXS) and the amide nitrogen of Ile369 form hydrogen bonds with the adenylate base N6 and N1, respectively. All three cofactor interactions mediated by the ArnA elements ($Helix_{326–337}$, $Loop_{347–349}$ and $Helix_{373–381}$) are conserved in the hUXS structures.

DISCUSSION

The Bifurcated Mechanism of hUXS Explains the Stimulatory Effect of Exogenous NAD^+

A previous study has reported that exogenous NAD^+ can increase hUXS activity by as much as 40%.[15] Given that recombinant hUXS purifies with a tightly bound NAD^+ cofactor, and the sequential oxidation and reduction steps of the catalytic cycle regenerate the cofactor (Figure 1),[16] the mechanism by which exogenous NAD^+ could stimulate activity was not clear. It has been proposed that heterologously expressed hUXS produces a significant amount of apoenzyme.[15] Thus, the stimulatory effect of exogenous NAD^+ is due to the apoenzyme binding cofactor. We have shown that our recombinant hUXS purifies with stoichiometric amounts of cofactor (Figure 2A). We also show that hUXS can catalytically produce NADH and UX4O in the presence of saturating NAD^+ and substrate (Figure 2). The use of CZE was key to observing the slow release of the reaction intermediates. Previous studies[18–21] relied on the lower resolution techniques HPLC or TLC to assay UXS, which makes the separation and identification of the UX4O intermediate difficult (Figure 3A,B). This suggests that HPLC should be used with caution in future studies of UXS and related SDR enzymes.[49] The release of the reaction intermediates implies a bifurcated mechanism in which the production of UX4O and NADH competes, albeit weakly, with the synthesis of UDX (Figure 4A). More importantly, the bifurcated scheme we propose offers a plausible explanation for the apparent stimulatory effect of exogenous NAD^+. In the absence of exogenous NAD^+, the hUXS:NADH: UX4O complex will be in dynamic equilibrium with apohUXS (Figure 4A). Thus, we expect a small fraction of hUXS to be losing the reduced cofactor during turnover, decreasing the apparent activity of the enzyme. In fact, we observe that at low protein concentrations, hUXS is unstable and loses activity (unpublished observations). Therefore, the apparent increase in activity in the presence of exogenous NAD^+ could be due to the rescue of apo-hUXS from an otherwise abortive catalytic cycle.

ArnA Conserves the Bifurcated Mechanism and Substrate Cooperativity of UXS

In ArnA, UDX production displays a lag in activity that is well modeled by Frieden's equation for transient kinetics (Figure 5B).[39] However, we do not believe the production of UDX by ArnA involves enzyme hysteresis. Instead, we note that the half-life of the lag coincides with high levels of the products NADH and UX4O and depletion of UGA (Figure 5C). We also observe that the production of UDX is reflected in the depletion of NADH and

UX4O. This suggests that the released products NADH and UX4O rebind to the ArnA active site to produce UDX. This is similar to a recent report of an ArnA-like protein that also rebinds NADH and UX4O to produce UDX.[50] The lag is likely due to the low concentrations of NADH and UX4O early in the progress curves, and the competition with UGA for the active site. The progress curves of NADH and UX4O production do not display a lag, effectively ruling out enzyme hysteresis as the source of the lag.

Our results show that the catalytic machinery for UDX synthesis is already present in ArnA. We believe that a fundamental difference between hUXS and ArnA is the equilibrium between E:NADH:UX4O and E* in the bifurcated mechanism, which acts as a catalytic shunt to favor one product over another (Figure 4A). In hUXS, the production of UX4O and NADH is ~2 orders of magnitude slower than UDX synthesis, indicating that the shunt favors the retention of the intermediates. In contrast, ArnA quickly releases UX4O and NADH, followed by a slower rate of UDX formation. Our data show that as the products UX4O and NADH accumulate in the ArnA reaction, E* is driven to the E:NADH:UX4O complex to produce UDX (Figures 4A and 5C). Thus, the equilibrium shunt favors the E:NADH:UX4O complex in hUXS, and the E* state in ArnA.

Gatzeva-Topalova et al. have proposed that the function of the hUXS $Loop_{120–124}$ is to retain NADH, and its absence in ArnA suggests a mechanism by which NADH could be released during the catalytic cycle.[22,33] Consistent with this proposal, truncation of the equivalent loop in UDP-galactose 4-epimerase (GalE) results in an E* form of GalE that reversibly binds NAD^+ during catalysis.[51] Our detailed structural analysis suggests that $Loop_{120–124}$ is but one small part of the catalytic shunt (Figures 4D and 7C). We have identified several structural elements that also contribute to the induced fit binding of cofactor and substrate (Figures 7 and 8). We believe that small changes in any of these elements are likely to influence the equilibrium between E:NADH:UX4O and E* in the bifurcated mechanisms of hUXS and ArnA.

Additional evidence that hUXS and ArnA share the same bifurcated mechanism comes from the cooperative binding of the cofactor in both enzymes (Figure 4). The observed cooperativity means that the conformational changes that occur upon binding of one NAD^+ molecule to the E* complex are reflected in the structure of the other subunit in the dimer. Our analysis of hUXS crystal structures indicates that significant local unfolding of the shunt is required to expose the active site and bind substrate (Figure 7C). Analysis of ArnA structures, which captures separate ArnA* and NAD^+-mimic bound conformations, reveals the structural elements associated with the induced fit conformational change that accompanies cofactor binding (Figure 8). Specifically, $Helix_{396–400}$ ($Helix_{165–168}$ in hXS) is positioned to interact with the N-termini of both dimer interface helices and might propagate cooperative binding in ArnA*. A crystal structure of hUXS* is currently unavailable. However, conservation of the cooperative conformational change in hUXS and ArnA suggests a common mechanism for communication between subunits using equivalent structural elements.

Acknowledgments

Funding

This work was supported in part by the Integrated Technology Resource for Biomedical Glycomics (P41RR018502, L.W. senior investigator). Funding from the American Cancer Society Research Scholar Grant (RSG0918401DMC) and the University of Georgia Research Alliance to Z.A.W. is gratefully acknowledged.

We thank Dr. Marcelo Sousa for the ArnA pMS159 construct. We also thank Dr. Maor Bar-Peled for the gift of the UDP-4-ketoxylose standard. The authors would additionally like to thank Dr. Debra Mohnen and the CarboSource Services facility for help with HPLC purification.

ABBREVIATIONS USED

hUXS	human UDP-xylose synthase
UGA	UDP-α-D-glucuronic acid
UX4O	UDP-α-D-4-keto-xylose
UDX	UDP-α-D-xylose
ArnA	*Escherichia coli* UDP-α-D-glucuronic acid decarboxylase
CZE	capillary zone electrophoresis
CID-MS^n	collision induced dissociation mass spectrometry
NSBD	nucleotide sugar binding domain
GalE	UDP-α-D-galactose 4-epimerase

REFERENCES

1. Esko JD, Selleck SB. Order out of chaos: assembly of ligand binding sites in heparan sulfate. Annu. Rev. Biochem. 2002; 71:435–471. [PubMed: 12045103]
2. Fuster MM, Esko JD. The sweet and sour of cancer: glycans as novel therapeutic targets. Nat. Rev. Cancer. 2005; 5:526–542. [PubMed: 16069816]
3. Lamoureux F, Baud'huin M, Duplomb L, Heymann D, Redini F. Proteoglycans: key partners in bone cell biology. Bioessays. 2007; 29:758–771. [PubMed: 17621645]
4. Esko JD, Rostand KS, Weinke JL. Tumor formation dependent on proteoglycan biosynthesis. Science. 1988; 241:1092–1096. [PubMed: 3137658]
5. Belting M, Borsig L, Fuster MM, Brown JR, Persson L, Fransson LA, Esko JD. Tumor attenuation by combined heparan sulfate and polyamine depletion. Proc. Natl. Acad. Sci. U. S. A. 2002; 99:371–376. [PubMed: 11752393]
6. Bai X, Zhou D, Brown JR, Crawford BE, Hennet T, Esko JD. Biosynthesis of the linkage region of glycosaminoglycans: cloning and activity of galactosyltransferase II, the sixth member of the beta 1,3-galactosyltransferase family (beta 3GalT6). J. Biol. Chem. 2001; 276:48189–48195. [PubMed: 11551958]
7. Silbert JE, Sugumaran G. Biosynthesis of chondroitin/dermatan sulfate. IUBMB Life. 2002; 54:177–186. [PubMed: 12512856]
8. Sugahara K, Kitagawa H. Heparin and heparan sulfate biosynthesis. IUBMB Life. 2002; 54:163–175. [PubMed: 12512855]
9. Rampal R, Luther KB, Haltiwanger RS. Notch signaling in normal and disease states: possible therapies related to glycosylation. Curr. Mol. Med. 2007; 7:427–445. [PubMed: 17584081]

10. Takeuchi H, Fernandez-Valdivia RC, Caswell DS, Nita-Lazar A, Rana NA, Garner TP, Weldeghiorghis TK, Macnaughtan MA, Jafar-Nejad H, Haltiwanger RS. Rumi functions as both a protein O-glucosyltransferase and a protein O-xylosyltransferase. Proc. Natl. Acad. Sci. U. S. A. 2011; 108:16600–16605. [PubMed: 21949356]
11. de Bernabe DB, Inamori K, Yoshida-Moriguchi T, Weydert CJ, Harper HA, Willer T, Henry MD, Campbell KP. Loss of alpha-dystroglycan laminin binding in epithelium-derived cancers is caused by silencing of LARGE. J. Biol. Chem. 2009; 284:11279–11284. [PubMed: 19244252]
12. Inamori K, Yoshida-Moriguchi T, Hara Y, Anderson ME, Yu L, Campbell KP. Dystroglycan function requires xylosyland glucuronyltransferase activities of LARGE. Science. 2012; 335:93–96. [PubMed: 22223806]
13. Filling C, Berndt KD, Benach J, Knapp S, Prozorovski T, Nordling E, Ladenstein R, Jornvall H, Oppermann U. Critical residues for structure and catalysis in short-chain dehydrogenases/reductases. J. Biol. Chem. 2002; 277:25677–25684. [PubMed: 11976334]
14. Kallberg Y, Oppermann U, Jornvall H, Persson B. Short-chain dehydrogenases/reductases (SDRs). Eur. J. Biochem./FEBS. 2002; 269:4409–4417.
15. Eixelsberger T, Sykora S, Egger S, Brunsteiner M, Kavanagh KL, Oppermann U, Brecker L, Nidetzky B. Structure and mechanism of human UDP-xylose synthase: evidence for a promoting role of sugar ring distortion in a three-step catalytic conversion of UDP-glucuronic acid. J. Biol. Chem. 2012; 287:31349–31358. [PubMed: 22810237]
16. Eames BF, Singer A, Smith GA, Wood ZA, Yan YL, He X, Polizzi SJ, Catchen JM, Rodriguez-Mari A, Linbo T, Raible DW, Postlethwait JH. UDP xylose synthase 1 is required for morphogenesis and histogenesis of the craniofacial skeleton. Dev. Biol. 2010; 341:400–415. [PubMed: 20226781]
17. John KV, Schwartz NB, Ankel H. UDP-glucuronate carboxy-lyase in cultured chondrocytes. J. Biol. Chem. 1977; 252:6707–6710. [PubMed: 197101]
18. Bar-Peled M, Griffith CL, Doering TL. Functional cloning and characterization of a UDP-glucuronic acid decarboxylase: the pathogenic fungus Cryptococcus neoformans elucidates UDP-xylose synthesis. Proc. Natl. Acad. Sci. U. S. A. 2001; 98:12003–12008. [PubMed: 11593010]
19. Harper AD, Bar-Peled M. Biosynthesis of UDP-xylose. Cloning and characterization of a novel Arabidopsis gene family, UXS, encoding soluble and putative membrane-bound UDP-glucuronic acid decarboxylase isoforms. Plant Physiol. 2002; 130:2188–2198. [PubMed: 12481102]
20. Kobayashi M, Nakagawa H, Suda I, Miyagawa I, Matoh T. Purification and cDNA cloning of UDP-D-glucuronate carboxy-lyase (UDP-d-xylose synthase) from pea seedlings. Plant Cell Physiol. 2002; 43:1259–1265. [PubMed: 12461125]
21. Pattathil S, Harper AD, Bar-Peled M. Biosynthesis of UDP-xylose: characterization of membrane-bound AtUxs2. Planta. 2005; 221:538–548. [PubMed: 15655675]
22. Gatzeva-Topalova PZ, May AP, Sousa MC. Crystal structure of Escherichia coli ArnA (PmrI) decarboxylase domain. A key enzyme for lipid A modification with 4-amino-4-deoxy-l-arabinose and polymyxin resistance. Biochemistry. 2004; 43:13370–13379. [PubMed: 15491143]
23. Breazeale SD, Ribeiro AA, Raetz CR. Oxidative decarboxylation of UDP-glucuronic acid in extracts of polymyxin-resistant Escherichia coli. Origin of lipid a species modified with 4-amino-4-deoxy-l-arabinose. J. Biol. Chem. 2002; 277:2886–2896. [PubMed: 11706007]
24. Hald E, Lehmann P, Ziegenhorn J. Molar Absorptivities of β-NADH and β-NAD at 260 nm. Clin. Chem. 1975; 21:884–887. [PubMed: 165910]
25. Gasteiger, E.; Hoogland, C.; Gattiker, A.; Duvaud, S.; Wilkins, MR.; Appel, RD.; Bairoch, A. Protein Identification and Analysis Tools on the ExPASy Server. In: Walker, JM., editor. The Proteomics Protocols Handbook. Totowa, NJ: Humana Press; 2005. p. 571-607.
26. Otwinowski Z, Minor W. Processing of X-ray diffraction data collected in oscillation mode. Methods Enzymol. 1996; 276:307–326.
27. Kabsch W. Xds. Acta Crystallogr., Sect. D. 2010; 66:125–132. [PubMed: 20124692]
28. Brunger AT, Adams PD, Clore GM, DeLano WL, Gros P, Grosse-Kunstleve RW, Jiang JS, Kuszewski J, Nilges M, Pannu NS, Read RJ, Rice LM, Simonson T, Warren GL. Crystallography and NMR system: A new software suite for macromolecular structure determination. Acta Crystallogr., Sect. D. 1998; 54:905–921. [PubMed: 9757107]

29. Brunger AT. Free R Value: Cross-validation in Crystallography. Methods Enzymol. 1997; 277B: 366–396. [PubMed: 18488318]
30. Collaborative Computational Project, N. The CCP4 suite: programs for protein crystallography. Acta Crystallogr., Sect. D. 1994; 50:760–763. [PubMed: 15299374]
31. Emsley P, Cowtan K. Coot: model-building tools for molecular graphics. Acta Crystallogr., Sect. D. 2004; 60:2126–2132. [PubMed: 15572765]
32. Williams GJ, Breazeale SD, Raetz CR, Naismith JH. Structure and function of both domains of ArnA, a dual function decarboxylase and a formyltransferase, involved in 4-amino-4-deoxy-l-arabinose biosynthesis. J. Biol. Chem. 2005; 280:23000–23008. [PubMed: 15809294]
33. Gatzeva-Topalova PZ, May AP, Sousa MC. Structure and mechanism of ArnA: conformational change implies ordered dehydrogenase mechanism in key enzyme for polymyxin resistance. Structure. 2005; 13:929–942. [PubMed: 15939024]
34. Altschul SF, Gish W, Miller W, Myers EW, Lipman DJ. Basic local alignment search tool. J. Mol. Biol. 1990; 215:403–410. [PubMed: 2231712]
35. Holm L, Park J. DaliLite workbench for protein structure comparison. Bioinformatics. 2000; 16:566–567. [PubMed: 10980157]
36. Wallace AC, Laskowski RA, Thornton JM. LIGPLOT: a program to generate schematic diagrams of protein-ligand interactions. Protein Eng. 1995; 8:127–134. [PubMed: 7630882]
37. Richards FM, Kundrot CE. Identification of structural motifs from protein coordinate data: secondary structure and first-level supersecondary structure. Proteins. 1988; 3:71–84. [PubMed: 3399495]
38. Hayward S, Berendsen HJ. Systematic analysis of domain motions in proteins from conformational change: new results on citrate synthase and T4 lysozyme. Proteins. 1998; 30:144–154. [PubMed: 9489922]
39. Frieden C. Kinetic aspects of regulation of metabolic processes. The hysteretic enzyme concept. J. Biol. Chem. 1970; 245:5788–5799. [PubMed: 5472372]
40. Zhang XJ, Wozniak JA, Matthews BW. Protein flexibility and adaptability seen in 25 crystal forms of T4 lysozyme. J. Mol. Biol. 1995; 250:527–552. [PubMed: 7616572]
41. Dickerson RE, Goodsell DS, Neidle S. ″…the tyranny of the lattice…″. Proc. Natl. Acad. Sci. U. S. A. 1994; 91:3579–3583. [PubMed: 8170950]
42. Wu Y, Lai DKW, Houk KN. Transition structures of hydride transfer reactions of protonated pyridinium ion with 1,4-dihydropyridine and protonated nicotinamide with 1,4-dihydronicotinamide. J. Am. Chem. Soc. 1995; 117:4100–4108.
43. Mesecar AD, Stoddard BL, Koshland DE Jr. Orbital steering in the catalytic power of enzymes: small structural changes with large catalytic consequences. Science. 1997; 277:202–206. [PubMed: 9211842]
44. Fraaije MW, Mattevi A. Flavoenzymes: diverse catalysts with recurrent features. Trends Biochem. Sci. 2000; 25:126–132. [PubMed: 10694883]
45. Allard ST, Beis K, Giraud MF, Hegeman AD, Gross JW, Wilmouth RC, Whitfield C, Graninger M, Messner P, Allen AG, Maskell DJ, Naismith JH. Toward a structural understanding of the dehydratase mechanism. Structure. 2002; 10:81–92. [PubMed: 11796113]
46. Naismith JH, Emmerich C, Habash J, Harrop SJ, Helliwell JR, Hunter WN, Raftery J, Kalb AJ, Yariv J. Refined structure of concanavalin A complexed with methyl alpha-D-mannopyranoside at 2.0 Å resolution and comparison with the saccharide-free structure. Acta Crystallogr., Sect. D. 1994; 50:847–858. [PubMed: 15299352]
47. Bouckaert J, Hamelryck TW, Wyns L, Loris R. The crystal structures of Man(alpha1–3)Man(alpha1-O)Me and Man(alpha1–6)Man(alpha1-O)Me in complex with concanavalin A. J. Biol. Chem. 1999; 274:29188–29195. [PubMed: 10506175]
48. Kadirvelraj R, Foley BL, Dyekjaer JD, Woods RJ. Involvement of water in carbohydrate-protein binding: concanavalin A revisited. J. Am. Chem. Soc. 2008; 130:16933–16942. [PubMed: 19053475]
49. Xu G, Lehmann R, Schleicher E, Haring HU, Liebich H. Advantages in the analysis of UDP-sugars by capillary electrophoresis-comparison of the conventional HPLC method with two new

capillary electrophoretic micro-procedures. Biomed. Chromatogr. 1998; 12:113–115. [PubMed: 9646903]

50. Gu X, Glushka J, Yin Y, Xu Y, Denny T, Smith J, Jiang Y, Bar-Peled M. Identification of a bifunctional UDP-4-ketopentose/UDP-xylose synthase in the plant pathogenic bacterium Ralstonia solanacearum strain GMI1000, a distinct member of the 4,6-dehydratase and decarboxylase family. J. Biol. Chem. 2010; 285:9030–9040. [PubMed: 20118241]
51. Sakuraba H, Kawai T, Yoneda K, Ohshima T. Crystal structure of UDP-galactose 4-epimerase from the hyperthermophilic archaeon Pyrobaculum calidifontis. Arch. Biochem. Biophys. 2011; 512:126–134. [PubMed: 21645492]
52. Diederichs K, Karplus PA. Improved R-factors for diffraction data analysis in macromolecular crystallography. Nat. Struct. Biol. 1997; 4:269–275. [published erratum appears in *Nat. Struct. Biol.* 1997 Jul;4(7):592]. [PubMed: 9095194]

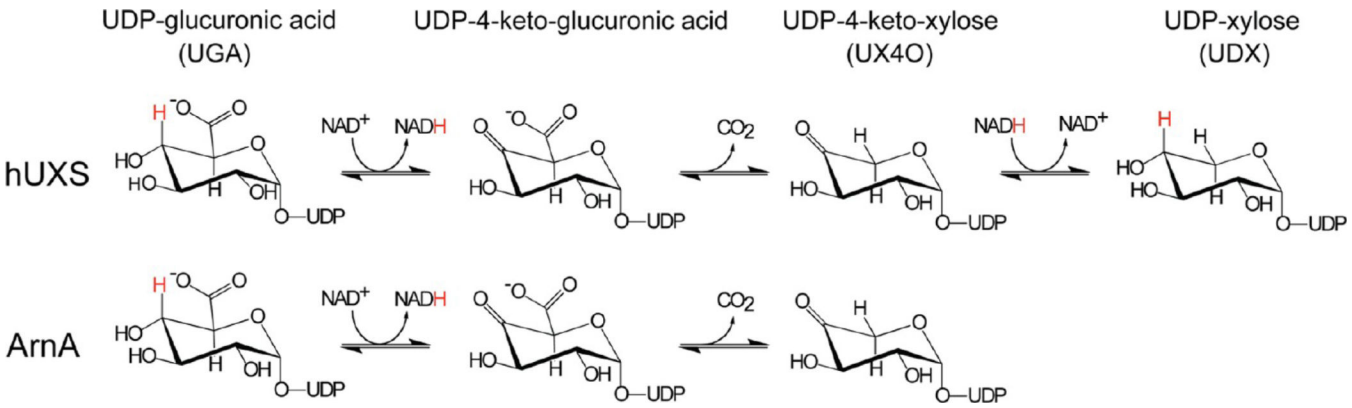

Figure 1.

UXS and ArnA have similar catalytic mechanisms. UDP-glucuronic acid (UGA) decarboxylases catalyze NAD^+-dependent oxidation of the C4′ position of substrate to form UDP-4-keto-xylose (UX4O) and NADH. ArnA releases UX4O and NADH as products. UXS retains UX4O and NADH as intermediates to form UDP-xylose (UDX). The C4′ proton involved in hydride transfer is depicted in red.

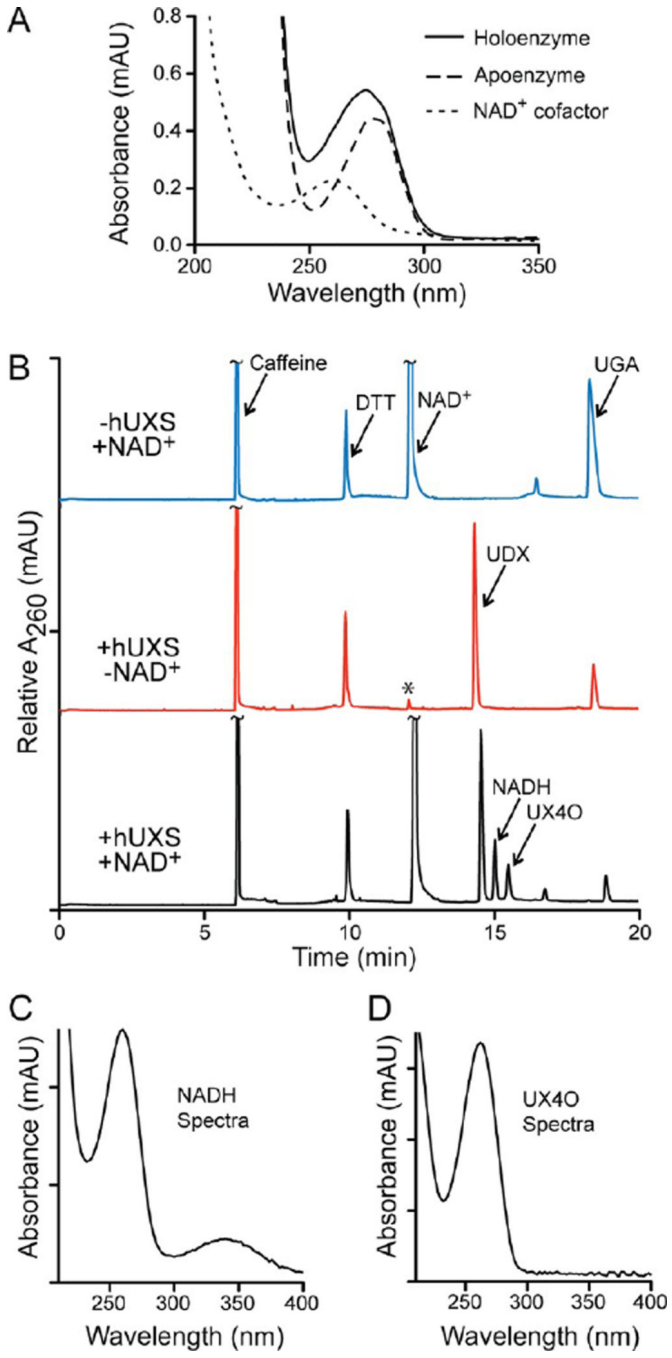

Figure 2.

hUXS releases UX4O and NADH in the presence of NAD^+. (A) Absorbance spectra of purified recombinant hUXS holoenzyme (solid line). Boiling releases NAD^+ cofactor (dotted line) in stoichiometric amounts with apoenzyme (dashed line). The apoenzyme spectrum was calculated as the difference between the total protein and NAD^+ spectra (see Methods). (B) Capillary zone electrophoresis (CZE) chromatogram of hUXS reaction with NAD^+ only (blue, upper trace), hUXS only (red, middle trace), or both NAD^+ and hUXS (black, lower trace). The bound NAD^+ cofactor in recombinant hUXS is depicted with an

asterisk (*). Absorbance spectra measured at 260 nm (A_{260}) are offset vertically and the caffeine standard and NAD^+ peaks have been truncated (~) for ease of viewing. (C) Absorbance spectra of NADH showing characteristic peaks at 260 and 340 nm and (D) UX4O showing a single peak at 262 nm consistent with the uridine moiety of UDP-sugars. Standard reactions with or without 2.5 mM NAD^+ and 1 mg/mL hUXS were incubated with 1 mM UGA at 37 °C and quenched with chloroform after 1 h.

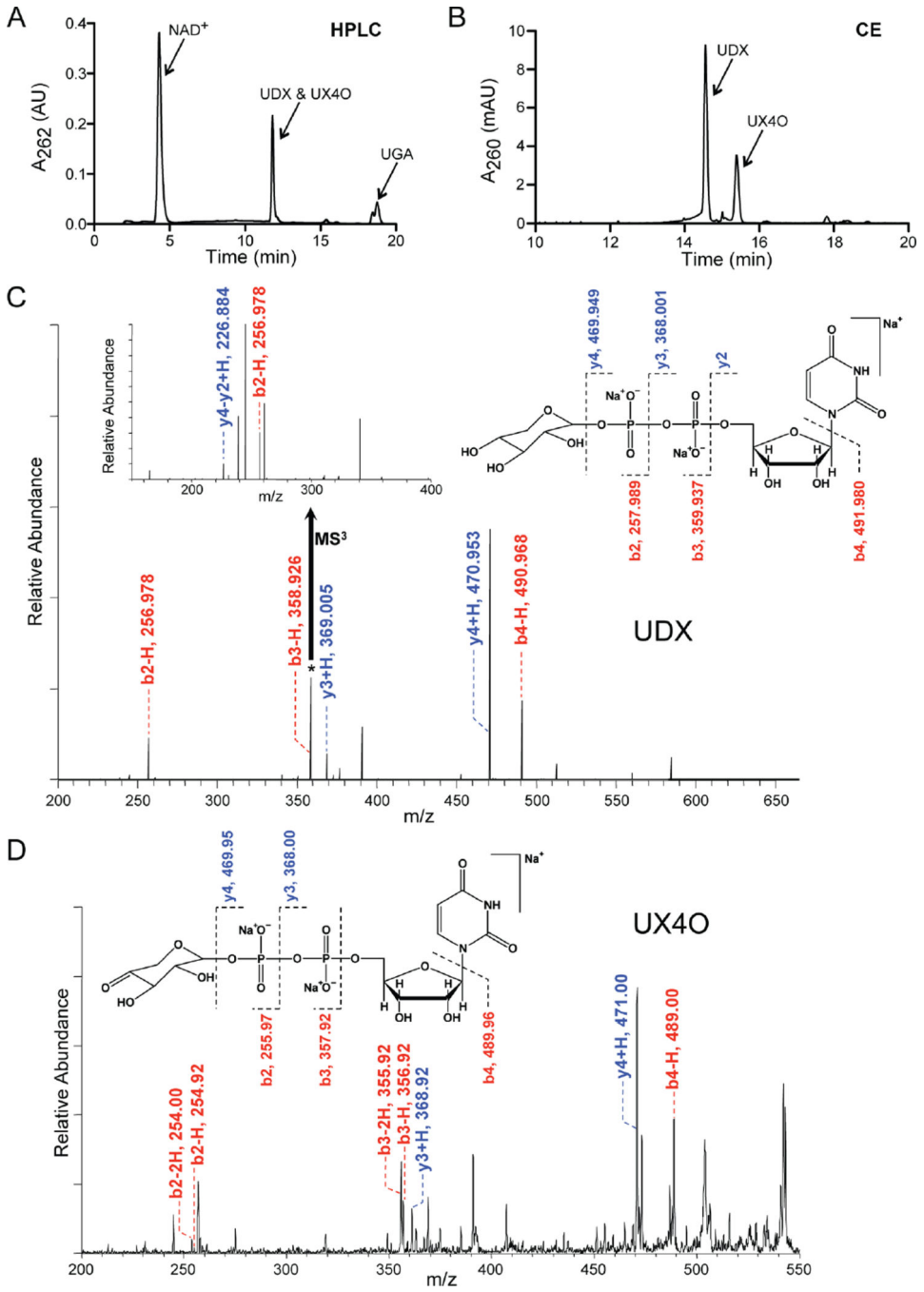

Figure 3.

Identification of UX4O. (A) HPLC chromatogram of the hUXS reaction showing UX4O and UDX comigrate as a single product peak between NAD^+ and UGA. (B) CZE chromatogram of the HPLC purified UDX fraction, confirming UX4O and UDX comigrate by HPLC but can be resolved with CZE. (C) Collision induced dissociation mass spectra ($CID\text{-}MS^n$) of the HPLC product peak, showing the major hUXS product is consistent with sodiated UDX and (D) the minor product corresponds to sodiated UX4O. Sodiated UDP-sugars are diagrammed to show the expected masses of the fragment ions before proton rearrangement.

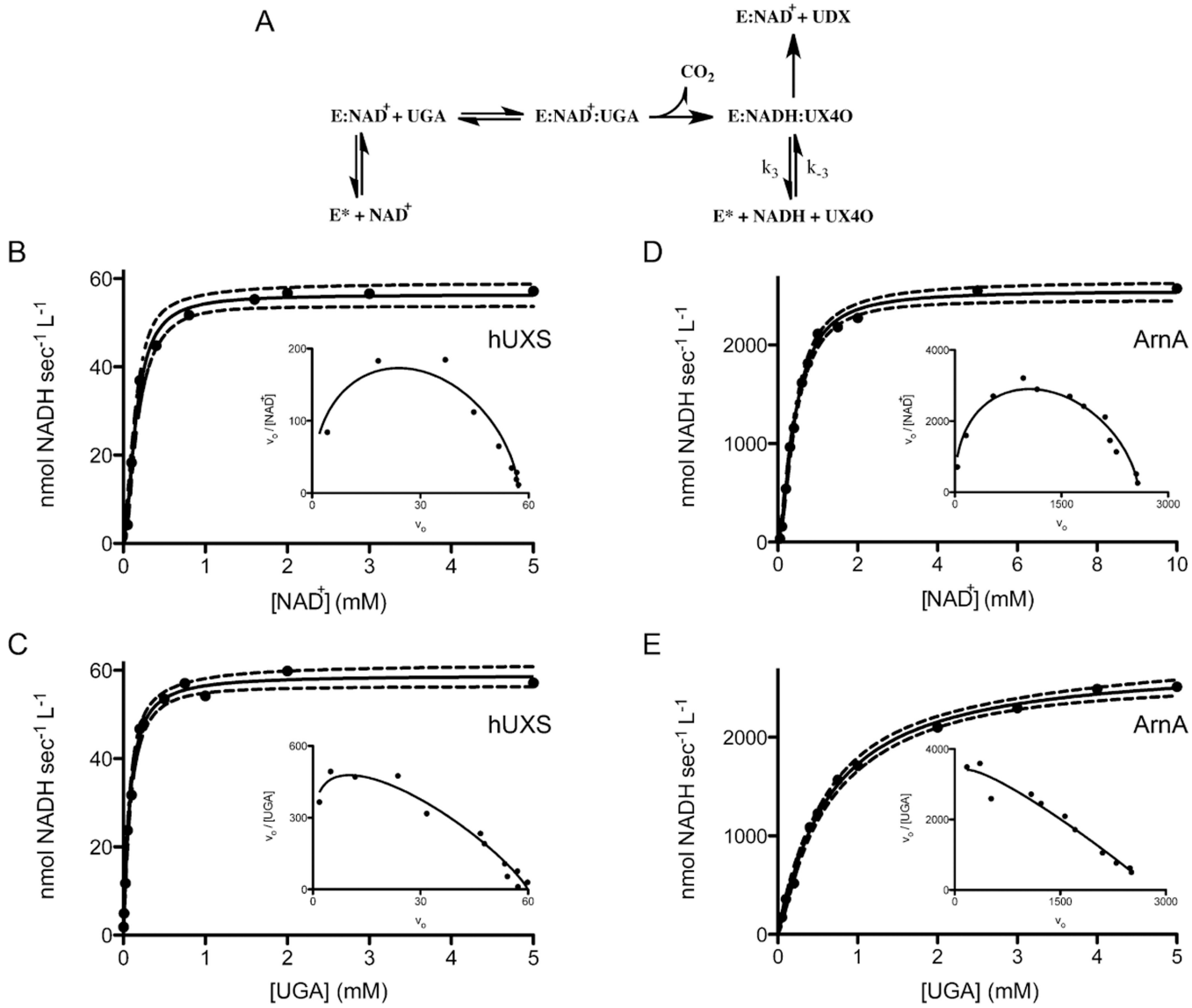

Figure 4.

Decarboxylase activities of hUXS and ArnA. (A) Bifurcated reaction scheme for UGA decarboxylases. hUXS purifies with NAD^+ bound ($E:NAD^+$). UGA binding results in formation of the Michaelis complex ($E:NAD^+:UGA$). UGA decarboxylation evolves CO_2 and leads to formation of the intermediate complex (E:NADH:UX4O). hUXS favors a second hydride transfer to form UDX, but can release the NADH and UX4O intermediates using a catalytic shunt (k_3). (B, C) Substrate saturation curves for hUXS release of NADH and UX4O. Initial velocity data were fit using nonlinear regression to the bifurcated rate equation (see Methods for derivation) and 95% confidence intervals (dashed lines) are depicted. Eadie-Scatchard plots (insets) are presented for illustrative purposes only. (D, E) Substrate saturation curves for ArnA release of NADH and UX4O depicted as above.

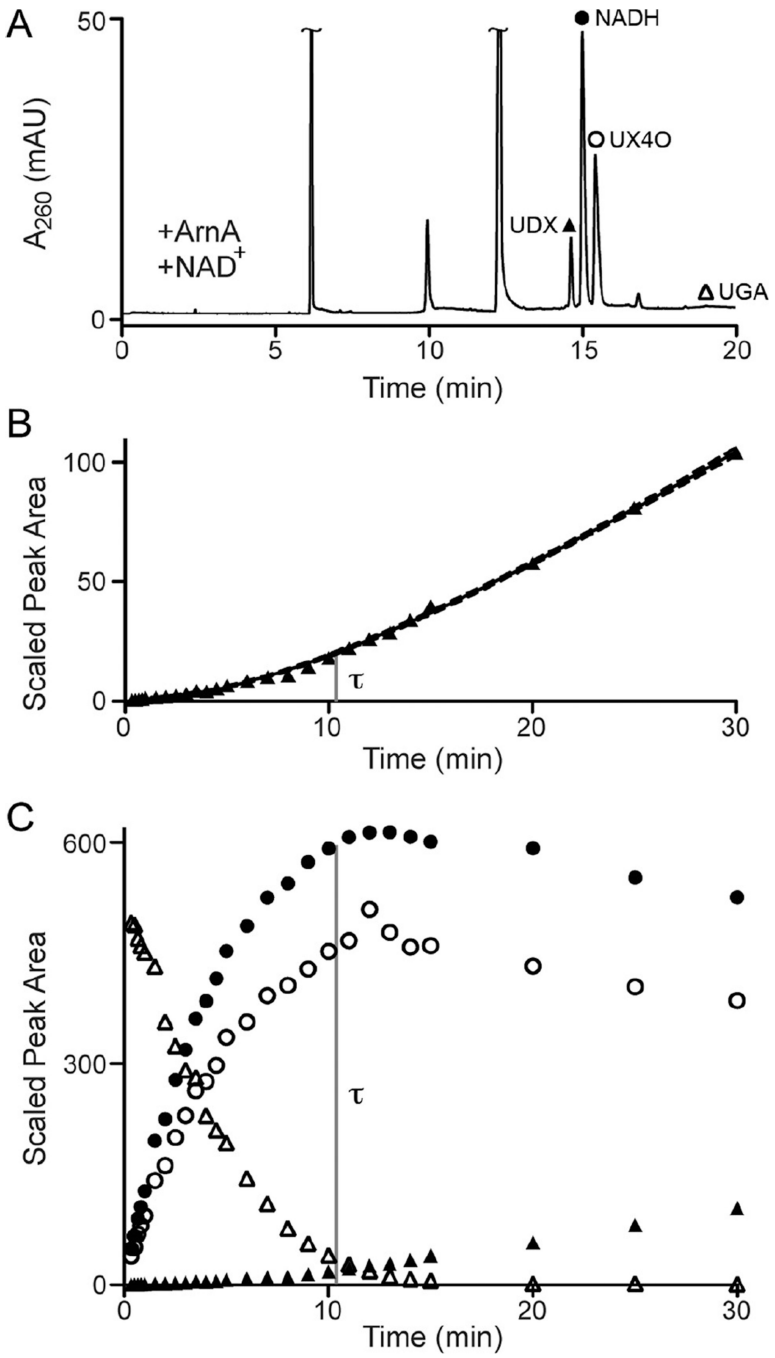

Figure 5.

ArnA catalyzes UDP-xylose synthesis. (A) CZE chromatogram of ArnA reaction showing UDX (▲), NADH (●) and UX4O (○) are produced from NAD^+ and UGA (△). Peaks were identified by comigration with known standards and caffeine and NAD^+ peaks are truncated (~) for ease of viewing. (B) Progress curve showing ArnA displays a lag in UDX production. UDX was resolved by CZE and product peaks were scaled using the internal caffeine standard. Data were fit by nonlinear regression to the equation of Frieden[39] and the half-life for the transition (τ) is denoted by a gray line. The 95% confidence interval (dashed

line) is narrow and superimposes with the curve and data points. (C) Progress curves of the ArnA reaction following all species labeled above. τ (gray line) is extrapolated to show production of UDX increases after UGA is depleted and UX4O and NADH accumulate.

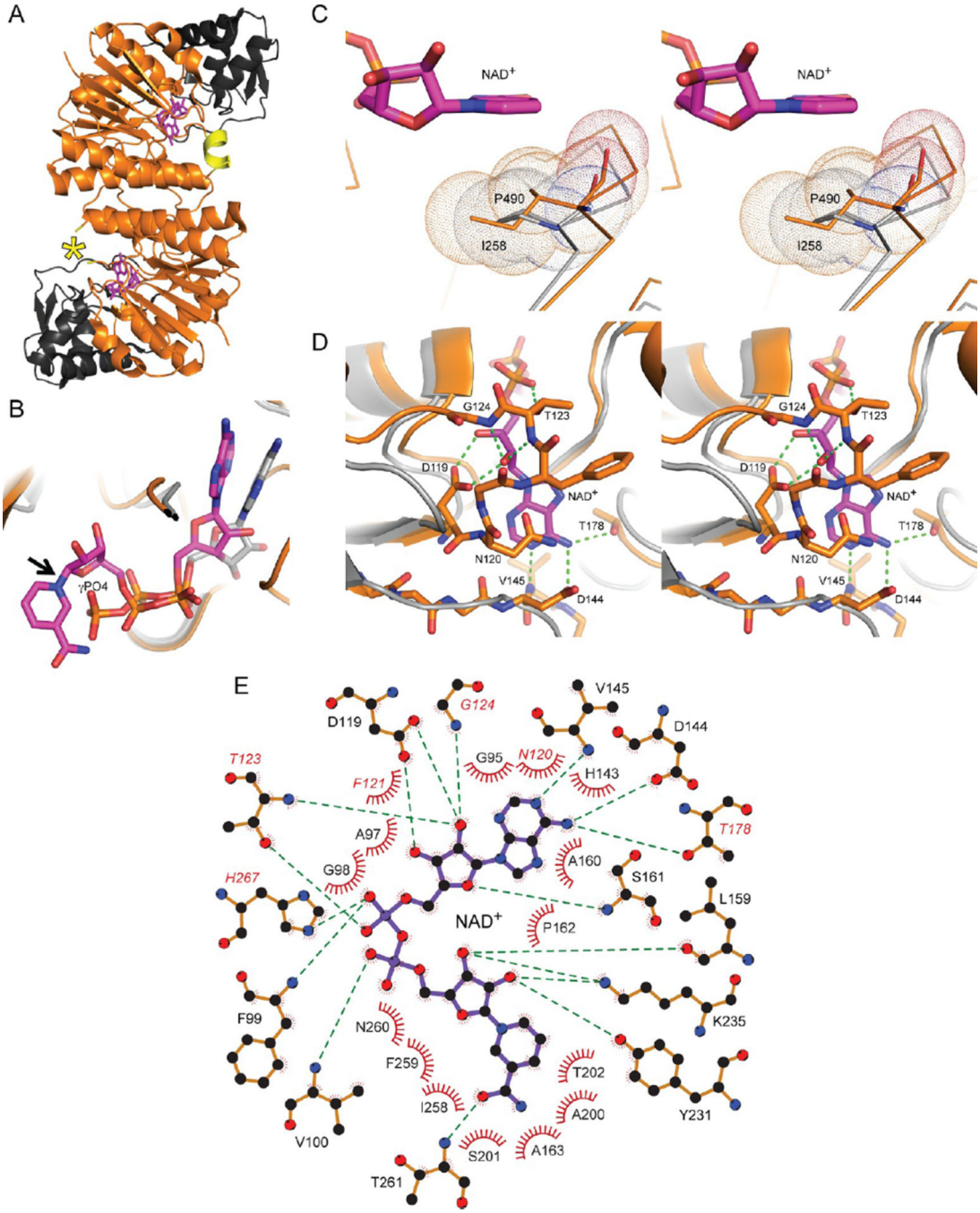

Figure 6.

NAD^+ is buried in the hUXS catalytic domain. (A) The dimeric structure of hUXS with the nucleotide sugar binding (NSBD) and catalytic domains identified (black and orange, respectively). $Helix_{165–168}$ (yellow) is ordered in one subunit and disordered in the other (yellow asterisk). NAD^+ (purple sticks) is depicted in the catalytic domain. (B) Structural overlay of hUXS (orange) and the ArnA:UGA:ATP complex (PDB entry 1Z7E, gray) showing the adenine bases in NAD^+ (purple) and ATP (gray) are bound in altered conformations, and the smaller γ-phosphate is nonisosteric with the nicotinamide ring and

ribose bound in hUXS. The NAD^+ χ_N torsion angle is identified (arrow). (C) Stereodiagram showing Ile258 from hUXS (orange) and Pro490 from ArnA (gray) form a similar van der Waals packing surface (dots) in the nicotinamide binding pocket. (D) Stereodiagram of the NAD^+ binding pockets of hUXS and ArnA colored as above to illustrate the hUXS cofactor binding $Loop_{120–124}$ and hydrogen bonding network (dashed lines). (E) Ligplot of hydrogen bonding interactions (dashed lines) and packing interactions (feathered lines) between hUXS and NAD^+. Red italics identify interactions in hUXS that are not present in ArnA.

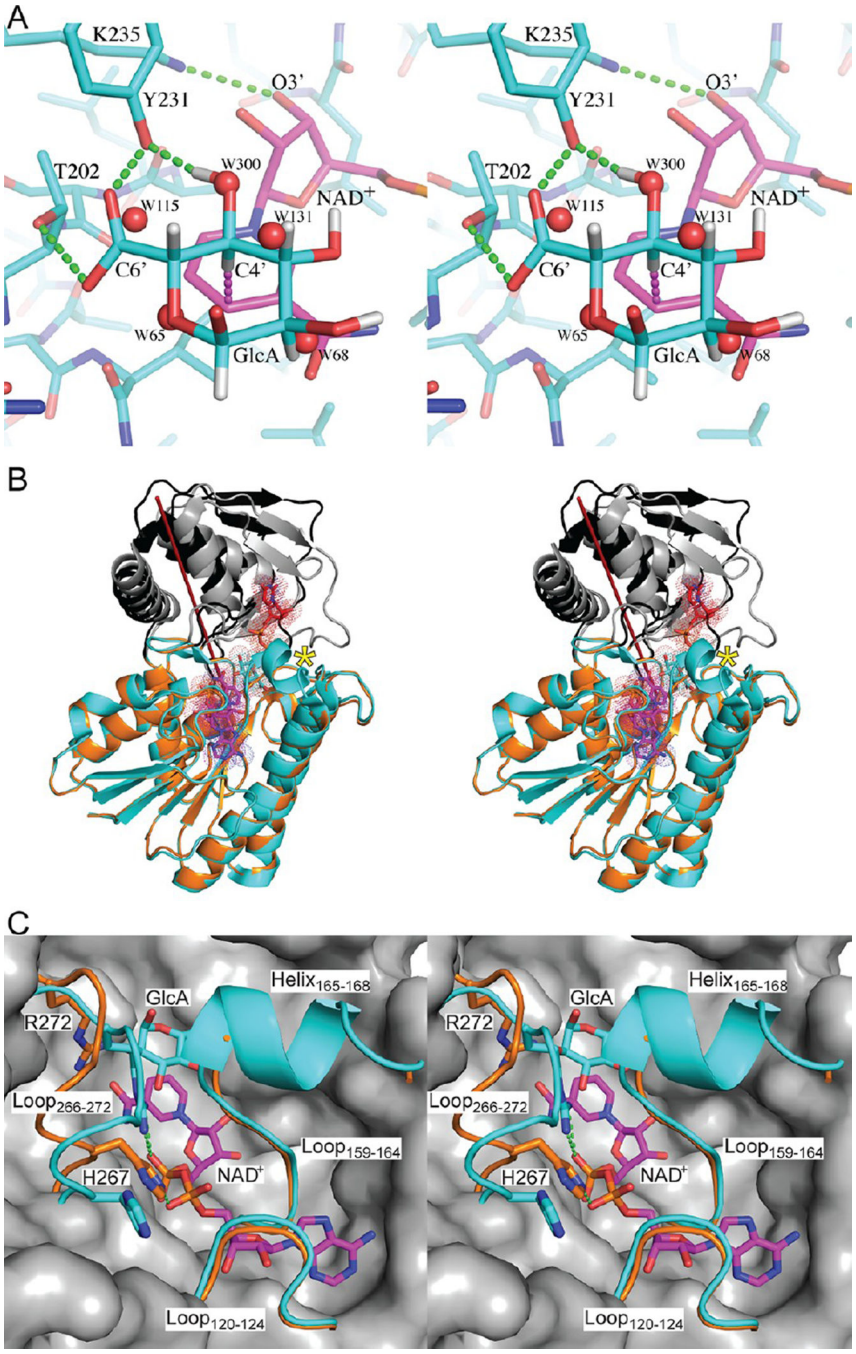

Figure 7.

UDP binding in hUXS induces conformational changes to the NSBD and active site. (A) Stereodiagram of the closed hUXS:UDP complex active site with GlcA modeled above the bound NAD^+ (purple). Carbon atoms C4′ and C6′ of the GlcA model are indicated, and hydrogens are included for clarity. Red spheres indicate the waters (labeled W) that occupy the active site in the absence of substrate. Hydrogen bonds are depicted as green dashes, and the path of hydride transfer from the sugar C4′ to the nicotinamide C4 is indicated by purple dashes. (B) Stereodiagram of the open hUXS monomer (orange with black NSBD) and

NAD^+ (purple sticks) superimposed onto closed hUXS (teal with gray NSBD) and UDP (red sticks). Van der Waal surfaces (dots) are shown for bound ligands and modeled GlcA (teal sticks). The DYNDOM[38] calculated axis about which the NSBD rotates is depicted as a red line and the disordered $Helix_{165–168}$ is labeled with an asterisk. (C) Stereodiagram of the open (orange) and closed (teal) hUXS active sites showing the catalytic shunt elements $Loop_{120–124}$, $Loop_{266–272}$, $Loop_{159–164}$ and $Helix_{165–168}$ relative to native NAD^+ cofactor (purple sticks) and modeled GlcA substrate (teal sticks). UDP binding stabilizes $Helix_{165–168}$ and induces R272 and H267 to change conformation, thereby altering the hydrogen bond (green dashes) network to the NAD^+ diphosphates. Chain B of open hUXS was used in the superposition to illustrate the effect of $Helix_{165–168}$ disorder on active site accessibility.

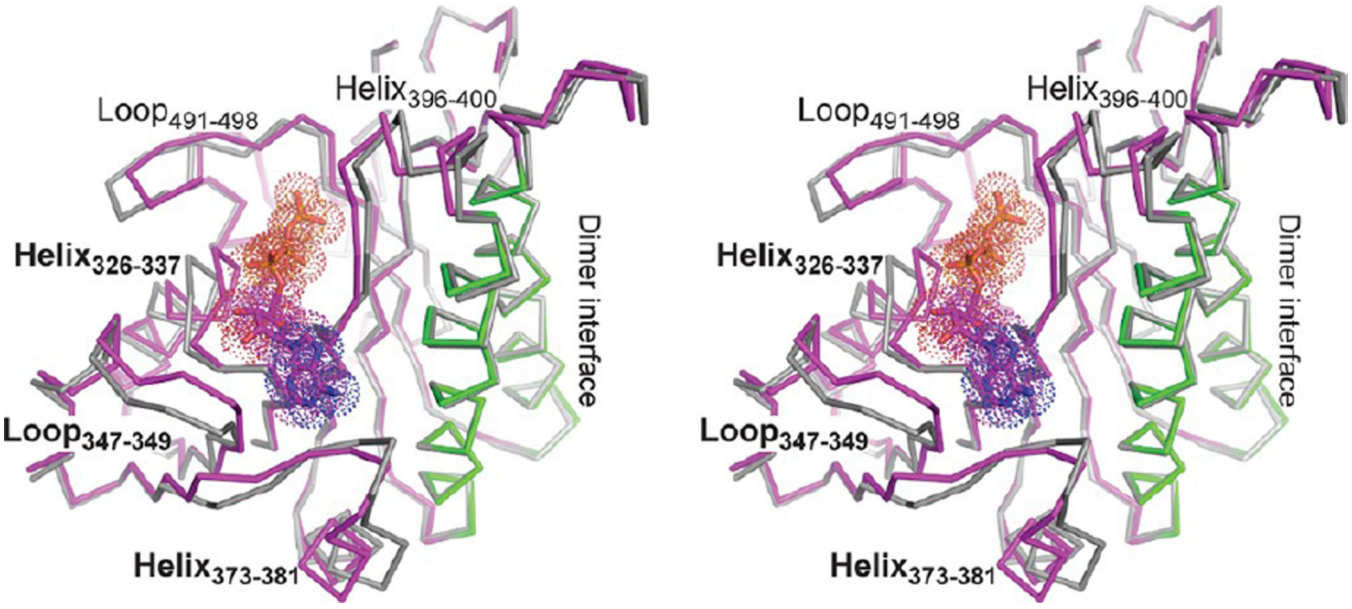

Figure 8.

Cofactor binding in ArnA induces additional conformational changes in the active site. Stereodiagram of the apo-ArnA (gray; PDB entry 2BLL) and ArnA:ATP:UGA (purple; PDB entry 1Z7E) catalytic domains showing the organization of mobile elements around the cofactor analog ATP (van der Waals spheres). ArnA $Helix_{396–400}$ and $Loop_{491–498}$ are analogous to hUXS $Helix_{165–168}$ and $Loop_{266–272}$, respectively (Figure 7C). Bold letters indicate elements in the cofactor binding site that undergo conformational changes not present in the hUXS crystal structures. The dimerization helices (green) and interface are labeled in the ArnA:ATP:UGA complex to indicate the proximity of mobile elements to the adjacent subunit.

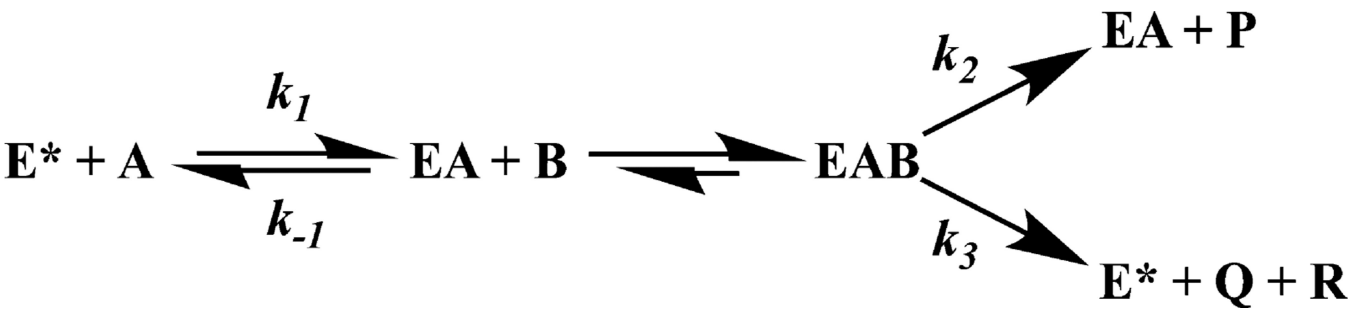

Scheme 1.

Table 1

Crystallographic Data and Refinement Statistics

data collection statistics		model refinement statistics	
wavelength (Å)	1.00	no. of amino acids	760
resolution (Å)	50–2.5	no. of NAD^+	2
total observations	343,332	no. of waters	146
unique reflections	30,682	total non-H atoms	5084
completeness (%)	97.3 (90)[a]	average B ($Å^2$)	39.7
multiplicity	11.2 (11.0)	*R*-factor	0.178 (0.227)
$<I/\sigma>$	26.2 (4.7)	free *R*-factor	0.223 (0.303)
R_{meas}[b]	8.3 (57.5)	stereochemical ideality	
$R_{mrgd\text{-}F}$[c]	6.4 (31.1)	bond length rmsd (Å)	0.014
		bond angle rmsd (°)	1.44
		φ,ψ most favored (%)	97.4
		φ,ψ allowed (%)	2.6

[a] Numbers in parentheses represent the highest resolution shell (2.57 to 2.5 Å).

[b] R_{meas} is the multiplicity weighted merging R-factor.[52]

[c] $R_{mrgd\text{-}F}$ is a measure of data accuracy.[52]

Table 2

Steady State Kinetic Parameters for UGA Decarboxylation Reactions

enzyme[a]	substrate dependence	kinetic property[b]	nonlinear regression best-fit value[c]
hUXS	NAD^+	V_{max}^{app}	56.4 ± 1.1
		h	1.76 ± 0.18
		K_M^{app}	155 ± 10
	UGA	V_{max}^{app}	58.9 ± 1.1
		h	1.22 ± 0.09
		K_M^{app}	75.8 ± 11.2
ArnA	NAD^+	V_{max}^{app}	2550 ± 43
		h	1.65 ± 0.09
		K_M^{app}	433 ± 16
	UGA	V_{max}^{app}	2755 ± 85
		h	1.10 ± 0.07
		K_M^{app}	623 ± 50

[a] Enzyme assays monitoring NADH absorbance at 340 nm were performed under standard conditions. hUXS (1 mg/mL) was incubated with varying NAD^+ (0.05−5 mM) and saturating UGA (1 mM) or varying UGA (0.005−5 mM) and saturating NAD^+ (5 mM). ArnA (0.5 mg/mL) was incubated with varying NAD^+ (0.05−15 mM) and saturating UGA (5 mM) or varying UGA (0.05−5 mM) and saturating NAD^+ (5 mM).

[b] Apparent maximum reaction velocity (V_{max}^{app}) is reported in nmol $L^{-1}s^{-1}$, the Hill coefficient (*h*) is unitless, and the apparent Michaelis constant (K_M^{app}) is reported in μM.

[c] Values were fit by nonlinear regression to the bifurcated rate equation (see Methods for derivation) as implemented in Prism.